Atomistic Modeling of Spin and Electron Dynamics in Two-Dimensional Magnets Switched by Two-Dimensional Topological Insulators

Sabyasachi Tiwari,[1,2,3] Maarten L. Van de Put,[1,3] Kristiaan Temst,[4] William G. Vandenberghe,[1,*] and Bart Sorée[3,5,6,†]

[1] *Department of Materials Science and Engineering, The University of Texas at Dallas, 800 W Campbell Road, Richardson, Texas 75080, USA*
[2] *Department of Materials Engineering, KU Leuven, Kasteelpark Arenberg 44, Leuven 3001, Belgium*
[3] *Imec, Kapeldreef 75, Heverlee 3001, Belgium*
[4] *Quantum Solid State Physics, Department of Physics and Astronomy, KU Leuven, Celestijnenlaan 200 D, Leuven B-3001, Belgium*
[5] *Department of Electrical Engineering, KU Leuven, Kasteelpark Arenberg 10, Leuven 3001, Belgium*
[6] *Department of Physics, University of Antwerp, Groenenborgerlaan 171, Antwerp 2020, Belgium*

(Received 1 April 2022; revised 10 October 2022; accepted 21 November 2022; published 12 January 2023)

To design fast memory devices, we need material combinations that can facilitate fast read and write operations. We present a heterostructure comprising a two-dimensional (2D) magnet and a 2D topological insulator (TI) as a viable option for designing fast memory devices. We theoretically model the spin-charge dynamics between 2D magnets and 2D TIs. Using the adiabatic approximation, we combine the nonequilibrium Green's function method for spin-dependent electron transport and a time-quantified Monte Carlo method for simulating magnetization dynamics. We show that it is possible to switch a magnetic domain of a ferromagnet using the spin torque from spin-polarized edge states of a 2D TI. We show further that the switching of 2D magnets by TIs is strongly dependent on the interface exchange (J_{int}), and an optimal interface exchange, is required for efficient switching. Finally, we compare experimentally grown Cr compounds and show that Cr compounds with higher anisotropy (such as CrI_3) result in a lower switching speed but a more stable magnetic order.

DOI: 10.1103/PhysRevApplied.19.014040

I. INTRODUCTION

Thanks to the recent discovery of two-dimensional (2D) magnets, e.g., CrI_3 [1], $CrBr_3$ [2], and $CrGeTe_3$ [3], research into 2D magnetics has garnered unprecedented attention. 2D magnetic materials open up a plethora of opportunities for their use in future applications in devices, including spintronics [4,5], valleytronics [6], and skyrmion [7]-based magnetic memories [8]. However, many of these devices require low-dimensional magnets interfaced with semiconductors to function as memory devices [9–11].

An interesting avenue for designing electronic devices using low-dimensional magnets lies in interfacing low-dimensional ferromagnets (FMs) with topological insulators (TIs) [9,10]. The surface states of topological insulators can act as spin channels with a high spin polarizability. Moreover, depending on the direction of the applied bias, the spin of the edge states can be switched thanks to spin-momentum locking [12].

Although there has been some experimental work on realizing magnetic devices using TI-FM interfaces [9–12], a solid theoretical understanding of the interfacial physics is absent. Most theoretical work has either investigated equilibrium TI-FM interfaces with a FM having a fixed magnetic orientation [13,14] or investigated the impact of magnetic materials on the topological order of a TI [15].

For the technological application of TI-FM material systems, it is necessary to understand how the motion of spin-polarized charge carriers in TIs impacts the spin dynamics of the FM and vice versa. To understand such a coupled spin-charge effect, it is necessary to model the coupled spin-charge dynamics of TIs and FMs. There has been recent theoretical work on modeling FM-semiconductor interfaces [16–18]; however, a major issue lies in the description of 2D magnets.

Most of the current methods use the Landau-Lifshitz-Gilbert (LLG) [19] equation to describe magnetization dynamics, coupled with quantum transport methodologies, e.g., the nonequilibrium Green's function (NEGF) [20]. The largest limitation lies in the magnetization dynamics of the magnetic material, because the micromagnetic

*william.vandenberghe@utdallas.edu
†bart.soree@imec.be

LLG equation assumes a continuous description of the magnetic structure [16]. There have been recent advances in the atomistic LLG equation [21]; however, addition of exchange anisotropy is difficult within the LLG equation. Exchange anisotropy plays a major role in determining the magnetic order of low-dimensional magnets [22–26] and is hard to include in the LLG equation; most frequently, a scalar approximation to the exchange interactions is assumed [27].

On the other hand, Monte Carlo (MC) simulations have been shown to be very accurate in predicting temperature-dependent observables for 2D magnets, taking into account the full anisotropy [22,23,28]. Unfortunately, MC simulations do not have a standard method of quantifying time to obtain time-dependent observables such as those related to magnetic switching. There has been previous work on quantifying time within MC simulations for systems with in-plane rotational invariance [29,30], called time-quantified Monte Carlo (TQMC) simulations. Thankfully, most of the 2D magnetic materials yet discovered experimentally have an in-plane rotational invariance, and TQMC simulations can be applied for such materials for magnetization dynamics.

We present a theoretical study of spin dynamics and spin-induced switching in a TI-FM heterostructure. We combine the nonequilibrium Green's function method for spin-dependent electron transport with a time-quantified Monte Carlo method for simulating magnetic systems. We use our method to study spin-induced switching in a heterostructure consisting of a two-dimensional topological insulator and a two-dimensional ferromagnet. We show that it is possible to change the magnetic domain structure in the ferromagnet using spin injection from the TI, which can be used to design high-speed memory devices. We then show that the switching can be achieved efficiently only for an optimal interfacial exchange interaction between the TI and FM. Finally, we compare the switching times for four experimentally grown Cr compounds, CrI_3, $CrBr_3$, $CrCl_3$, and $CrGeTe_3$. We show that the higher anisotropy of CrI_3 results in a much larger switching time compared with $CrBr_3$ and $CrCl_3$, which have lower anisotropy.

II. METHODOLOGY

A. The Heisenberg Hamiltonian

We model the 2D magnetic structure using the Heisenberg Hamiltonian [22]

$$H_m = -\frac{1}{2}\sum_{i\neq j} \mathbf{S}_i \cdot \mathbf{J}_{ij} \cdot \mathbf{S}_j + D\sum_i (S_i^z)^2, \tag{1}$$

where $\mathbf{S} = S^{\mathbf{x}}\mathbf{x} + S^{\mathbf{y}}\mathbf{y} + S^{\mathbf{z}}\mathbf{z}$ is the spin vector, with magnitude $|\mathbf{S}| = \sqrt{(S^{\mathbf{x}})^2 + (S^{\mathbf{y}})^2 + (S^{\mathbf{z}})^2}$. The exchange interaction strength $\mathbf{J}_{ij}$ between spins at sites i and j is a 3×3 tensor [23], whose parameters are obtained by fitting to density-functional-theory (DFT) calculations [22,23]. The second term in Eq. (1) is the single-ion anisotropy, with strength D. We assume in-plane rotational invariance for the 2D magnetic material, which leads to the Hamiltonian reducing to

$$H_m = \sum_{i,j} \frac{J_{ij}}{2}\left[\mathbf{S}_i\cdot\mathbf{S}_j + \Delta_{ij}\left(S_i^{\mathbf{z}}S_j^{\mathbf{z}} - S_i^{\mathbf{x}}S_j^{\mathbf{x}} - S_i^{\mathbf{y}}S_j^{\mathbf{y}}\right)\right] + D\sum_i (S_i^{\mathbf{z}})^2, \tag{2}$$

where the exchange anisotropy (Δ_{ij}) accounts for the distinct values of the in-plane and out-of-plane anisotropic exchange strengths $J_{ij}^{\mathbf{xx}} = J_{ij}^{\mathbf{yy}} = J_{ij}(1-\Delta_{ij})$ and $J_{ij}^{\mathbf{zz}} = J_{ij}(1+\Delta_{ij})$ [22], respectively. Moreover, we define the total magnetization per atom in the **x**, **y**, and **z** directions as

$$S_{\mathbf{z/y/x}} = \frac{1}{N_{\text{atom}}}\sum_i S_i^{\mathbf{z/y/x}}. \tag{3}$$

Here, N_{atom} is the total number of atoms.

B. Electronic Hamiltonian

We model the electronic structure of the topological insulators using a tight-binding Hamiltonian,

$$H_{\text{elec}} = -t\sum_{\langle r,r'\rangle,\alpha} c_{r,\alpha}^{\dagger}c_{r',\alpha} + i\Lambda_{\text{so}}\sum_{\langle\langle r,r'\rangle\rangle,\alpha,\beta} v_{r,r'}c_{r,\alpha}^{\dagger}\sigma_{\alpha,\beta}^{\mathbf{z}}c_{r',\beta}. \tag{4}$$

Here the first term, with coupling strength t, accounts for the nearest-neighbor hopping, $\langle r, r'\rangle$, between adjacent lattice sites r and r', with respective electron creation and annihilation operators $c_{r,\alpha}^{\dagger}$ and $c_{r',\beta}$. α and β represent spin degrees of freedom, i.e., $\alpha \in \{\uparrow,\downarrow\}$ and $\beta \in \{\uparrow,\downarrow\}$. The second term is the next-nearest-neighbor spin-orbit-coupling term, with strength Λ_{so}. $\sigma^{\mathbf{z}}$ is the z component of the Pauli matrices. The parameter $v_{r,r'}$ is $+1$ when the shortest next-nearest-neighbor path from r to r' with respect to atom r is clockwise, and -1 if it is counterclockwise.

C. Combined Hamiltonian

We combine the models for the Heisenberg Hamiltonian and the electronic Hamiltonian using the interaction

Hamiltonians

$$H'_m = J_{\text{int}} \sum_{r,i} \mathbf{m}_r \cdot \mathbf{S}_i, \tag{5a}$$

$$H'_{\text{elec}} = J^e_{\text{int}} \sum_{i,r,\alpha,\beta} c^\dagger_{r,\alpha} \mathbf{S}_i \cdot \boldsymbol{\sigma}_{\alpha,\beta} c_{r,\beta}. \tag{5b}$$

The interaction Hamiltonians describe the effective interaction between the magnet and the TI atoms, where the magnetic moment is localized on the transition-metal atoms. Here, J_{int} and J^e_{int} are the interface interactions at the semiconductor-FM interface. The electron magnetization, $\mathbf{m} = m^x\mathbf{x} + m^y\mathbf{y} + m^z\mathbf{z}$, is the expectation value of the Pauli spin matrix, $\boldsymbol{\sigma} = \sigma^x\mathbf{x} + \sigma^y\mathbf{y} + \sigma^z\mathbf{z}$. Explicitly, we calculate the electron magnetization $\mathbf{m}$ by taking the trace of the density matrix over the spin degrees of freedom,

$$\mathbf{m}(r) = \frac{\hbar\gamma}{4\pi} \text{Tr}[\boldsymbol{\sigma} \cdot \rho(r,r')]_{\text{spin}}, \tag{6}$$

with the electronic density matrix

$$\rho(r,r') = \int G^<(r,r',E)\, dE, \tag{7}$$

where $G^<(E)$ is the lesser Green's function. As is standard in the ballistic NEGF method, the lesser Green's function is obtained from $G^<(r,r',E) = A_L(r,r',E)f\,(E-\mu_L) + A_R(r,r',E)f\,(E-\mu_R)$. Here, $A_L(r,r',E)$ and $A_R(r,r',E)$ are the spectral functions for the left (L) and right (R) contacts, respectively, and μ_L and μ_R are the respective chemical potentials, with $f\,(E)$ being the Fermi-Dirac distribution function. The spectral functions are obtained using $A_{L/R} = G^r\Gamma_{L/R}G^a$, with $\Gamma_{L/R} = i(\Sigma_{L/R} - \Sigma^\dagger_{L/R})$. $G^r(E) = (E - H'_{\text{elec}} - \Sigma_L - \Sigma_R)^{-1}$ is the retarded Green's function. The advanced Green's function is $G^a = (G^r)^\dagger$. The contact self-energies $\Sigma_{L/R}$ are obtained using the quantum transmitting-boundary method (QTBM) [31,32]. Similarly to the case for the magnet, we define the magnetization per atom in the TI as

$$m_{\mathbf{z/y/x}} = \frac{1}{N^{\text{TI}}_{\text{atom}}} \sum_i m_i^{\mathbf{z/y/x}}. \tag{8}$$

Here, $N^{\text{TI}}_{\text{atom}}$ is the total number of atoms in the TI.

D. Magnetization dynamics and time quantification

To simulate the magnetization dynamics as a function of time, we use the time-quantified MC approach [29,30]. In the TQMC method, one step of a MC simulation is assigned a time step Δt, with

$$R^2 = \frac{20k_BT\alpha\gamma}{(1+\alpha^2)M}\,\Delta t. \tag{9}$$

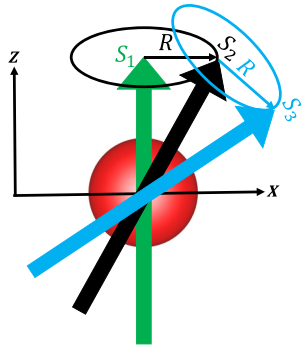

FIG. 1. Choice of spin in a MC step using the TQMC method. The spin S_1 shows the initial spin state, which can take a value within a radius R, with the spin state ranging between S_1 and S_2 (illustrated by the black circle). The spin state S_2 shows an intermediate spin state that can take a value within the radius R (illustrated in blue), with the spin state switching from S_2 to S_3. The radius R is determined by the Gilbert damping.

Here, R is a cone radius up to which a trial spin rotation is allowed in each MC step, k_B is the Boltzmann constant, α is the Gilbert damping parameter, $M = \sqrt{S^2_{\mathbf{x}} + S^2_{\mathbf{y}} + S^2_{\mathbf{z}}}$ is the magnetic moment, and γ is the gyromagnetic ratio.

Figure 1 shows a single magnetic atom, with spins chosen for three successive time steps using the TQMC method (S_1, S_2, S_3). In the TQMC method, for each time step, we make a cone of radius R around the spin vector of the present spin configuration (S_1, green). The next spin configuration (S_2, black) is chosen within the cone using the Metropolis algorithm [23,33]. Once the spin configuration has been updated to S_2, we choose the next spin configuration (S_3, blue) by using the same method of making a cone of radius R around S_2.

The expression in Eq. (9) for time discretization is obtained by assuming only single-spin interactions and Langevin dynamics [29,30]. Therefore, this time discretization is valid only under the condition that the magnetization dynamics can be approximated using Langevin dynamics, and is more accurate for materials with in-plane rotational invariance and Gilbert damping, i.e. $\alpha \leq 1$ [29,30]. The approximation of the magnetization dynamics by Langevin dynamics is valid only for a high out-of-plane anisotropy or very low temperatures ($T < 10$ K), where the spins start behaving collectively as a single unit. For this reason, we perform all our calculations below $T < 10$ K.

E. Algorithm for spin-charge dynamics

The energy of the magnetic interaction is of the order of millielectronvolts, while the electronic interaction energy

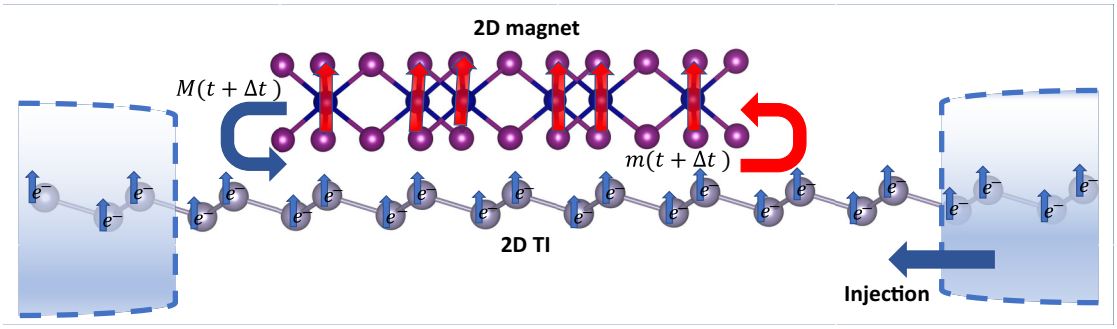

FIG. 2. Interface between a 2D TI and a layered magnet. Electrons are injected from the contacts (illustrated by the blue arrow below the right contact) at time $t+\Delta t$. The flowing electrons carry a small magnetic moment (illustrated by the small blue arrows), exerting a torque due to the electronic magnetic configuration $m(t+\Delta t)$ on the interfaced magnet, with magnetic configuration $M(t+\Delta t)$ (illustrated by the red arrows).

is of the order of electronvolts. Therefore, the time scales of the magnetization dynamics are measured in picoseconds, whereas that of the electrons is measured in femtoseconds. Within the adiabatic approximation, we assume that, due to the large differences in the time scales, the electrons can be considered to see only an adiabatic change in magnetic moment and are thus always found to occupy instantaneous eigenstates.

Hence, as shown in Fig. 2, we start with a magnetic orientation of the magnetic material, and at each time step $(t+\Delta t)$, we rotate the spin of the top magnetic layer using MC sampling. After the MC step, we calculate the magnetic moment of the magnet, $M(t+\Delta t)$. For the same time step, we obtain the lesser Green's function using the NEGF method and calculate the electronic magnetization $m(t+\Delta t)$. For the next time step, the magnetization of the electronic system is an input to the magnetic system, and the loop continues.

F. Computational details

For all calculations, unless otherwise mentioned specifically, we use the values $\alpha = 0.05$, $k_BT = 0.5$ meV, and $J_{\text{int}} = J^e_{\text{int}} = 25$ meV. We use a sharp pulse (the pulse immediately transitions to the applied voltage) in all our calculations. We use the parameters of a CrI_3 monolayer to parameterize the interfaced 2D ferromagnet, which we obtain from DFT calculations using the procedure in Ref. [22]. The saturation magnetization used for the Cr atoms is $3\mu_B$. To model the TI, we use the parameters of the tight-binding Hamiltonian for stanene [32].

III. RESULTS AND DISCUSSION

A. TI-FM interface operations

Figure 3(a) shows the TI-FM configuration that we investigate. For the TI, we use a 5-nm-wide stanene ribbon, and for the 2D FM, we use CrI_3 with size 3×3.5 nm. The 2D FM is positioned near one of the edges of the 2D TI, as shown in the top view in Fig. 3(a.2). A potential (V_{DS}) is applied across the TI ribbon to inject charge carriers into the TI ribbon. For $V_{DS} > 0$, the edge states on the top edge of the TI have an up spin, whereas the bottom edge exhibits a down spin. For $V_{DS} < 0$, the spin polarization of the edge states is flipped. Therefore, the interfaced

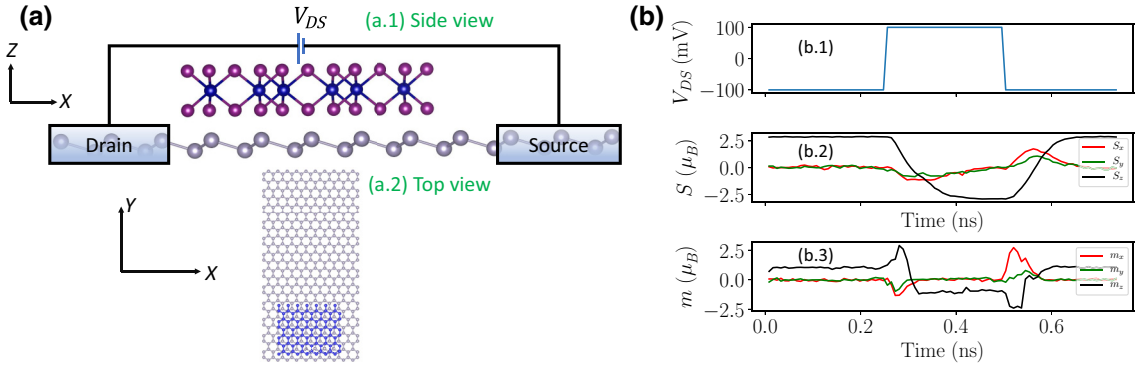

FIG. 3. (a) Device configuration studied for TI-FM switching. The 2D TI is contacted with a drain and a source contact, and a voltage (V_{DS}) is applied between the contacts. (b) Magnetization of the 2D FM as a function of time. (b.1) The bias is applied at $t = 0$ ns and switched to 100 meV from -100 meV at 0.25 ns. (b.2) The magnetization of the 2D FM in the **z** direction (S_z) switches its direction (from $3\mu_B$ to $-3\mu_B$). (b.3) Induced magnetization in the 2D TI.

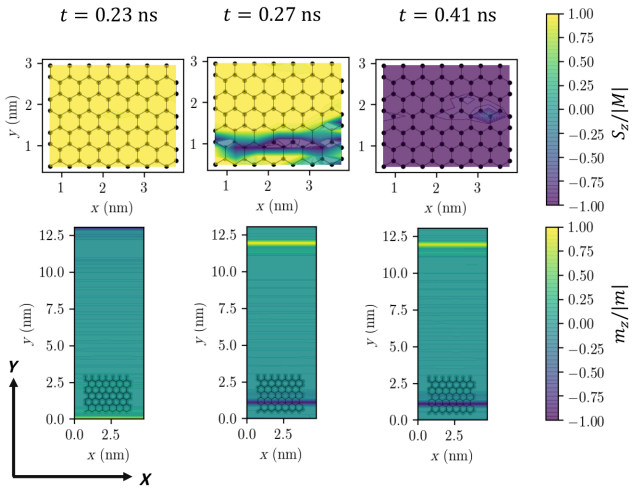

FIG. 4. Magnetic configuration $[M(t)]$ of the FM (upper three panels) and the electronic spin configuration $[m(t)]$ of the TI (lower three panels) at $t = 0.23$, 0.27, and 0.41 ns when the voltage pulse is switched at $t = 0.25$ ns. The atomic structure of the FM is shown superimposed on the magnetic configuration of the TI.

FM experiences a positive or negative spin torque from the underlying charge carriers in the TI, depending on the applied V_{DS}.

Figure 3(b.1) shows the applied V_{DS} as a function of time. We apply a step V_{DS} pulse of 100 mV at $t = 1.75$ ns. Figure 3(b.2) shows the average magnetization in the **x**, **y**, and **z** directions of the top FM layer as a function of the applied V_{DS}. We observe that with a change in the applied V_{DS} from -100 to 100 mV at $t = 0.5$ ns, the magnetization in the **z** direction (S_z) switches from $3\mu_B$ to $-3\mu_B$. When the applied voltage switches from 100 to -100 mV, we observe that the magnetization switches back from $-3\mu_B$ to $3\mu_B$. A similar operation using a pulsed voltage is presented in Fig. S1 in the Supplemental Material [34].

Figure 3(b.3) shows the induced magnetization of the TI ribbon in the **x**, **y**, and **z** directions as a function of time. We observe that, due to the magnetization of the top FM, there is a finite induced magnetization in the TI ribbon when the applied bias is nonzero. Interestingly, we find that whenever the bias switches and the magnetization of the top FM transitions, the total induced magnetization of the TI ribbon also shows a peak.

To further analyze the magnetization dynamics of the TI-FM interface, we plot the out-of-plane projection of the magnetization of the entire TI and FM sample at various time steps in Fig. 4. Figure 4 shows the magnetization in the **z** direction for the 2D magnet (top panels, $S_z/|M|$) and the TI (bottom panels, $m_z/|M|$). We observe that at $t = 0.23$ ns, the TI has a positive bias $V_{DS} > 0$ and both the TI and the FM have a positive magnetization at the interface. Note that we take the interface parameter to be positive, meaning that the interaction is ferromagnetic.

At $t = 0.27$ ns, the bias on the TI has the opposite polarization, $V_{DS} < 0$. We observe that the magnetization of the TI reverses. The reversal of the magnetization in the TI induces a spin torque on the interfaced FM, which results in the formation of a small region of magnetization with an opposite orientation to that of the rest of the FM ($\hat{S}_z < 0$). The peak of the magnetization as shown is delocalized slightly for the 2D TI ribbon due to the finite size, as well as to the position of the chosen Fermi level.

At $t = 0.41$ ns, we observe that the domain with $\hat{S}_z < 0$ grows and changes completely to a FM configuration, with the magnetization of the 2D magnet equal to $-3\mu_B$. Interestingly, we find that the top magnetization of the FM does not have a significant impact on the magnetization of the TI. The reason for such behavior is because we assume in our calculations an interface interaction strength $J_{\text{int}} = J^e_{\text{int}} = 25$ meV. The interaction strength felt by the TI is of the order of millielectronvolts, whereas the topological energy gap of the TI is of the order of electronvolts. Hence, the weak interaction strength always leads to a negligible response of the TI magnetization due to the magnetization at the interface with the FM (see Sec. III B for further discussion).

B. Impact of J_{int} and α

Figure 5(a.1) shows the applied bias across the 2D TI. We apply a V_{DS} pulse with a pulse width of 0.4 ns and an amplitude of 100 mV at $t = 0.8$ ns. Figure 5(a.2) shows the normalized magnetization of the interface 2D FM in the **z** direction ($S_z/|M|$) as a function of time for Gilbert damping parameters $\alpha = 0.02, 0.03, 0.04, 0.05$ and a pulse bias. With the transition in the applied V_{DS}, the normalized magnetization of the 2D magnet transitions from 1 to -1. We also observe that with increasing α, the transition occurs faster, suggesting that the switching speed increases.

Figures 5(b.1) and 5(b.2) show a pulse bias applied across the 2D TI with a pulse width of 0.2 ns applied at 0.4 ns as a function of time, and the normalized magnetization in the **z** direction ($S_z/|M|$) as a function of time for the interface 2D FM with interface exchange parameters $J_{\text{int}} = 5$, 25, 50, 100, and 150 meV. We observe that with increasing J_{int}, the transition occurs faster up to $J_{\text{int}} = 50$ meV. For $J_{\text{int}} > 50$ meV, we see that the magnetization does not switch smoothly, and the magnetization stabilizes for the entire duration of the pulse. After the applied pulse returns to 0 mV, the magnetization still switches for all $J_{\text{int}} > 50$ meV, albeit with some delay.

The magnetization of the interfaces when $J_{\text{int}} < 50$ mV shows a transition after the pulse is switched to zero. Because the magnetization induced by the TI induces a preferred direction, the magnet transitions from 1 to -1. However, in certain cases when the magnetization induced by the TI is smaller, the magnetic transition after the pulse

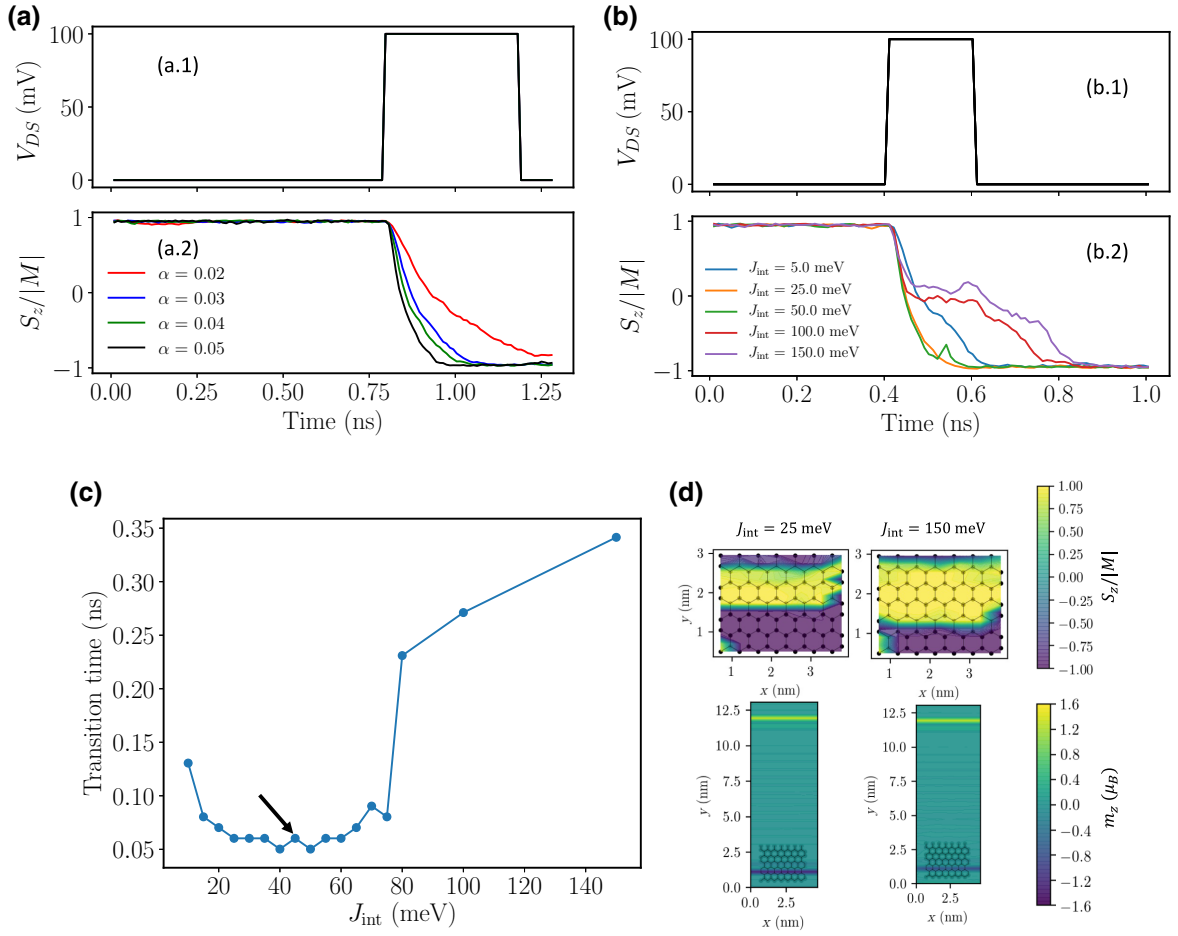

FIG. 5. (a) Applied V_{DS} (a.1) and the magnetization of the top 2D FM for $\alpha = 0.02, 0.03, 0.04, 0.05$ (a.2). (b) Applied V_{DS} and the magnetization of the top 2D FM for interface interaction strengths $J_{\text{int}} = 5, 25, 50, 100, 150$ meV (b.2). (c) Transition time for the applied pulse in (b.1) as a function of J_{int}. (d) Magnetization at $t = 0.45$ ns for $J_{\text{int}} = 25$ and 150 meV. The upper two panels show the magnetization of the 2D FM in the **z** direction ($S_z/|M|$), and the lower two panels show the induced magnetization in the 2D TI (m_z).

is removed can be random (more information is given in the Supplemental Material [34]).

Figure 5(c) shows the transition time for the applied pulse in Fig. 5(b.1) as a function of J_{int}. We define the transition time as $t[S_z < -0.7M] - t[S_z > 0.7M]$. We observe that the transition time decreases down as a function of J_{int} up to $J_{\text{int}} = 50$ meV and then increases for $J_{\text{int}} > 50$ meV. Therefore, we find that an optimal value of the interface exchange (J_{int}) exists.

To further understand the reason for the low transition rate at higher J_{int}, we compare the magnetization at $t = 0.45$ ns in Fig. 5(d) for $J_{\text{int}} = 25$ and 150 meV. The upper two panels show the magnetization of the 2D FM in the **z** direction ($S_z/|M|$), and the lower two panels show the induced magnetization in the 2D TI (m_z). We observe that for $J_{\text{int}} = 150$ meV, m_z is lower than the value of m_z for $J_{\text{int}} = 25$ meV. Therefore, the lower magnetization of the TI results in a lower torque on the 2D FM, causing a delay in the transition. The reason for the lower magnetization due to the higher J_{int} is because the magnet opens up a band gap in the 2D TI, resulting in a superposition of up and down spins [14]. The superposition of up and down spins in the TI leads to a reduced magnetization.

C. Impact of anisotropy and Cr compounds

We compare the transition time for the device in Fig. 3(a) as a function of the nearest-neighbor anisotropy (Δ_{NN}) of the FM, as shown in Fig. 6. We perform the same sweep of Δ_{NN} for ten different starting configurations. The solid line shows the median, and the shaded region shows the 25th–75th percentile. We use $J_{\text{int}} = 0.025$ eV and $\alpha = 0.05$ and take the nearest-neighbor exchange for the 2D magnet to be $J_{\text{NN}} = 2.5$ meV.

We find that with increasing Δ_{NN}, the transition time increases. Therefore, for faster switching of the TI-FM device, it would be ideal to use materials with a lower Δ_{NN}. However, a lower Δ_{NN} results in a lower Curie temperature [22]. Hence, the choice of the FM material should take

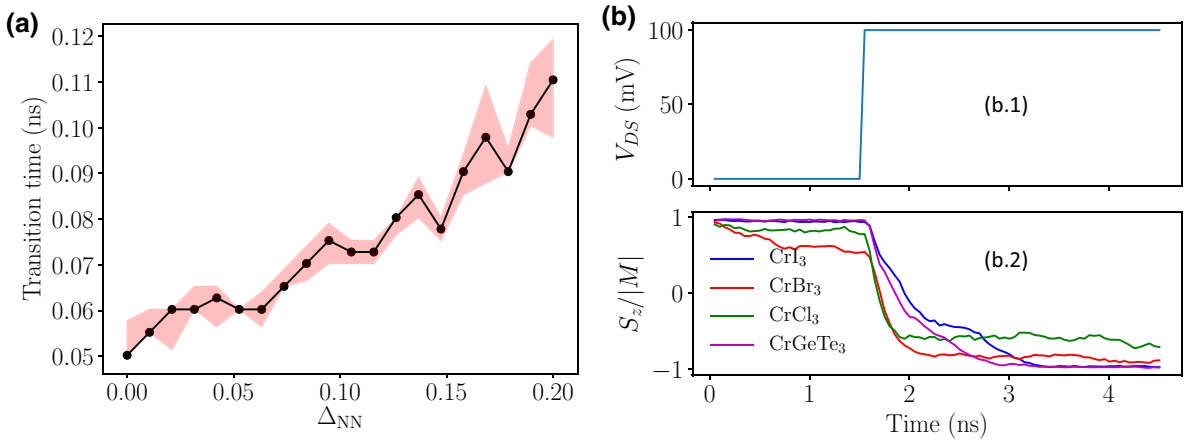

FIG. 6. (a) Transition time as a function of nearest-neighbor anisotropy Δ_{NN}. We perform the same sweep of Δ_{NN} for ten different starting configurations. The solid line shows the median, and the shaded region shows the 25th–75th percentile. (b) Comparison of switching in CrI_3, $CrBr_3$, $CrCl_3$, and $CrGeTe_3$. (b.1) Applied V_{DS}; (b.2) magnetization ($S_z/|M|$) for CrI_3, $CrBr_3$, $CrCl_3$, and $CrGeTe_3$. We use an interface exchange $J_{int} = 25$ meV, and $\alpha = 0.005$.

into account the temperature of operation and the required switching time of the device.

For the device shown in Fig. 3(a), we use CrI_3, $CrBr_3$, $CrCl_3$, and $CrGeTe_3$ as the 2D magnetic material. Although many previous studies have used a parametric value of α [35] for Cr compounds, recent reports on the measurement of the intrinsic Gilbert damping of the sister compound $CrCl_3$ have found a value of $\alpha = 0.002$ [36]. Unfortunately, there have been no similar reports for other Cr compounds; therefore, we use an α of similar order, $\alpha = 0.005$, for all three Cr compounds for a fair comparison. The parameters used for modeling the magnetic structure of the Cr compounds are shown in Table I.

Figure 6(b.1) shows the applied V_{DS}, and Fig. 6(b.2) shows the out-of-plane magnetization $S_z/|M|$ for CrI_3, $CrBr_3$, $CrCl_3$, and $CrGeTe_3$. The α used for the calculations for Cr compounds is an order of magnitude smaller than the α used in previous calculations, resulting in the time scale being an order of magnitude higher. We find that the magnetization of CrI_3 is the most stable among the Cr compounds, followed by $CrGeTe_3$, $CrBr_3$, and $CrCl_3$ (at times above 3 ns). However, CrI_3 is also the slowest to respond to a change in the applied bias and has the highest transition time. The fluctuations in the magnetic moment of the 2D magnets in the absence of an electric field are the result of thermal fluctuations at finite temperature.

TABLE I. J parameters and anisotropies of experimental Cr compounds.

Parameters	J_{NN} (meV)	J_{NNN} (meV)	J_{NNNN} (meV)	Δ_{NN}	Δ_{NNN}	Δ_{NNNN}
CrI_3	2.21	0.75	···	0.029	0.045	···
$CrBr_3$	1.38	0.44	···	0.010	0.012	···
$CrCl_3$	1.31	0.24	···	0.001	0.008	···
$CrGeTe_3$	5.87	−0.28	0.345	0.02	0.0	0.028

Comparing the parameters for the Cr compounds in Table I, we find that the transition time is inversely proportional to the nearest-neighbor anisotropy (Δ_{NN}). The higher the anisotropy, the higher the transition time. On the other hand, the stability of the magnetization is directly proportional to the anisotropy.

IV. CONCLUSION

We presented a method to model spin-charge dynamics at a magnetic–topological-insulator interface. Our model is general and not limited to only a TI-FM interface. Our method combines the NEGF and the TQMC method to model the spin-charge dynamics. The benefit of the TQMC+NEGF method over conventional methods such as the LLG+NEGF method lies in the atomistic description of the spins, which allows one to implement the full exchange tensor to model the magnetic exchange interactions.

Using our method, we theoretically investigated the spin-charge dynamics in a 2D TI-FM heterostructure where the size of the 2D FM is smaller than that of the 2D TI and the 2D FM is placed on one of the edges of the 2D TI. We showed that by electrically biasing the 2D TI, it is possible to switch the magnetization of the 2D FM without destroying the edge state of the 2D TI. The most important result of our work is that the switching of the 2D FM using a spin torque from the 2D TI can be achieved efficiently only in TI-FM material combinations that have an optimal interface exchange interaction J_{int}.

We also compared experimentally grown 2D Cr compounds. We showed that the transition rate of the magnetization depends significantly on the anisotropy, and the low-anisotropy Cr compounds ($CrBr_3$ and $CrCl_3$) show

faster switching than the higher-anisotropy Cr compounds (CrI_3 and $CrGeTe_3$). Finally, there have been recent reports of experimentally growing 2D FM-semiconductor heterostructures for spintronic devices [37]; given that the device design presented in our paper is feasible to make experimentally, we believe that it should be explored experimentally.

ACKNOWLEDGMENTS

The project and work presented here were sponsored by the Department of Defense, Defense Threat Reduction Agency. The content of the information does not necessarily reflect the position or the policy of the U.S. Federal Government, and no official endorsement should be inferred.

This material is based upon work supported by the National Science Foundation under Grant No. 1802166.

We thank the Research Foundation Flanders (FWO) and the KU Leuven BOF Program (C14/18/074). This work was supported by imec's Industrial Affiliation Program.

[1] B. Huang, G. Clark, E. Navarro-Moratalla, D. R. Klein, R. Cheng, K. L. Seyler, D. Zhong, E. Schmidgall, M. A. McGuire, D. H. Cobden, W. Yao, D. Xiao, P. Jarillo-Herrero, and X. Xu, Layer-dependent ferromagnetism in a van der Waals crystal down to the monolayer limit, Nature **546**, 270 EP (2017).

[2] Z. Zhang, J. Shang, C. Jiang, A. Rasmita, W. Gao, and T. Yu, Direct photoluminescence probing of ferromagnetism in monolayer two-dimensional $CrBr_3$, Nano Lett. **19**, 3138 (2019).

[3] C. Gong, L. Li, Z. Li, H. Ji, A. Stern, Y. Xia, T. Cao, W. Bao, C. Wang, Y. Wang, Z. Q. Qiu, R. J. Cava, S. G. Louie, J. Xia, and X. Zhang, Discovery of intrinsic ferromagnetism in two-dimensional van der Waals crystals, Nature **546**, 265 EP (2017).

[4] D. L. Cortie, G. L. Causer, K. C. Rule, H. Fritzsche, W. Kreuzpaintner, and F. Klose, Two-dimensional magnets: Forgotten history and recent progress towards spintronic applications, Adv. Funct. Mater. **30**, 1901414 (2020).

[5] Z. Wang, I. Gutiérrez-Lezama, N. Ubrig, M. Kroner, M. Gibertini, T. Taniguchi, K. Watanabe, A. Imamoğlu, E. Giannini, and A. F. Morpurgo, Very large tunneling magnetoresistance in layered magnetic semiconductor CrI_3, Nat. Commun. **9**, 2516 (2018).

[6] D. Zhong, K. L. Seyler, X. Linpeng, R. Cheng, N. Sivadas, B. Huang, E. Schmidgall, T. Taniguchi, K. Watanabe, M. A. McGuire, W. Yao, D. Xiao, K.-M. C. Fu, and X. Xu, Van der Waals engineering of ferromagnetic semiconductor heterostructures for spin and valleytronics, Sci. Adv. **3**, e1603113 (2017).

[7] D. Amoroso, P. Barone, and S. Picozzi, Spontaneous skyrmionic lattice from anisotropic symmetric exchange in a Ni-halide monolayer, Nat. Commun. **11**, 5784 (2020).

[8] Q. Tong, F. Liu, J. Xiao, and W. Yao, Skyrmions in the moiré of van der Waals 2D magnets, Nano Lett. **18**, 7194 (2018).

[9] Y. Fan, P. Upadhyaya, X. Kou, M. Lang, S. Takei, Z. Wang, J. Tang, L. He, L.-T. Chang, M. Montazeri, G. Yu, W. Jiang, T. Nie, R. N. Schwartz, Y. Tserkovnyak, and K. L. Wang, Magnetization switching through giant spin–orbit torque in a magnetically doped topological insulator heterostructure, Nat. Mater. **13**, 699 (2014).

[10] Y. Wang, D. Zhu, Y. Wu, Y. Yang, J. Yu, R. Ramaswamy, R. Mishra, S. Shi, M. Elyasi, K.-L. Teo, Y. Wu, and H. Yang, Room temperature magnetization switching in topological insulator-ferromagnet heterostructures by spin-orbit torques, Nat. Commun. **8**, 1364 (2017).

[11] J. Han, A. Richardella, S. A. Siddiqui, J. Finley, N. Samarth, and L. Liu, Room-Temperature Spin-Orbit Torque Switching Induced by a Topological Insulator, Phys. Rev. Lett. **119**, 077702 (2017).

[12] Y. Fan, X. Kou, P. Upadhyaya, Q. Shao, L. Pan, M. Lang, X. Che, J. Tang, M. Montazeri, K. Murata, L.-T. Chang, M. Akyol, G. Yu, T. Nie, K. L. Wong, J. Liu, Y. Wang, Y. Tserkovnyak, and K. L. Wang, Electric-field control of spin–orbit torque in a magnetically doped topological insulator, Nat. Nanotechnol. **11**, 352 (2016).

[13] S. Rachel and M. Ezawa, Giant magnetoresistance and perfect spin filter in silicene, germanene, and stanene, Phys. Rev. B **89**, 195303 (2014).

[14] J. S. Van Dyke and D. K. Morr, Effects of defects and dephasing on charge and spin currents in two-dimensional topological insulators, Phys. Rev. B **95**, 045151 (2017).

[15] Y. Hou, J. Kim, and R. Wu, Magnetizing topological surface states of Bi_2Se_3 with a CrI_3 monolayer, Sci. Adv. **5**, eaaw1874 (2019).

[16] J. Osca and B. Sorée, Skyrmion spin transfer torque due to current confined in a nanowire, Phys. Rev. B **102**, 125436 (2020).

[17] J. Osca and B. Sorée, Torque field and skyrmion motion by spin transfer torque in a quasi-2d interface in presence of strong spin–orbit interaction, J. Appl. Phys. **130**, 133903 (2021).

[18] J. Osca, K. Moors, B. Sorée, and L. Serra, Fabry–Pérot interferometry with gate-tunable 3D topological insulator nanowires Nanotechnology **32**, 435002 (2021).

[19] L. Landau and E. Lifshitz, in *Perspectives in Theoretical Physics*, edited by L. Pitaevski (Pergamon, Amsterdam, 1992), p. 51.

[20] M. D. Petrović, B. S. Popescu, U. Bajpai, P. Plecháč, and B. K. Nikolić, Spin and Charge Pumping by a Steady or Pulse-Current-Driven Magnetic Domain Wall: A Self-Consistent Multiscale Time-Dependent Quantum-Classical Hybrid Approach, Phys. Rev. Appl. **10**, 054038 (2018).

[21] R. F. L. Evans, W. J. Fan, P. Chureemart, T. A. Ostler, M. O. A. Ellis, and R. W. Chantrell, Atomistic spin model simulations of magnetic nanomaterials, J. Phys.: Condens. Matter **26**, 103202 (2014).

[22] S. Tiwari, J. Vanherck, M. L. Van de Put, W. G. Vandenberghe, and B. Sorée, Computing Curie temperature of two-dimensional ferromagnets in the presence of exchange anisotropy, Phys. Rev. Res. **3**, 043024 (2021).

[23] S. Tiwari, M. L. Van de Put, B. Sorée, and W. G. Vandenberghe, Critical behavior of the ferromagnets CrI_3, $CrBr_3$,

and $CrGeTe_3$ and the antiferromagnet $FeCl_2$: A detailed first-principles study, Phys. Rev. B **103**, 014432 (2021).

[24] J. Vanherck, B. Sorée, and W. Magnus, Anisotropic bulk and planar Heisenberg ferromagnets in uniform, arbitrarily oriented magnetic fields, J. Phys.: Condens. Matter **30**, 275801 (2018).

[25] J. Vanherck, C. Bacaksiz, B. Sorée, M. V. Milošević, and W. Magnus, 2D ferromagnetism at finite temperatures under quantum scrutiny, Appl. Phys. Lett. **117**, 052401 (2020).

[26] S. Tiwari, M. L. Van de Put, B. Sorée, and W. G. Vandenberghe, Magnetic order and critical temperature of substitutionally doped transition metal dichalcogenide monolayers, Npj 2D Mater. Appl. **5**, 54 (2021).

[27] X.-X. Zhang, L. Li, D. Weber, J. Goldberger, K. F. Mak, and J. Shan, Gate-tunable spin waves in antiferromagnetic atomic bilayers, Nat. Mater. **19**, 838 (2020).

[28] J. L. Lado and J. Fernández-Rossier, On the origin of magnetic anisotropy in two dimensional CrI_3, 2D Materials **4**, 035002 (2017).

[29] O. Chubykalo, U. Nowak, R. Smirnov-Rueda, M. A. Wongsam, R. W. Chantrell, and J. M. Gonzalez, Monte Carlo technique with a quantified time step: Application to the motion of magnetic moments, Phys. Rev. B **67**, 064422 (2003).

[30] U. Nowak, R. W. Chantrell, and E. C. Kennedy, Monte Carlo Simulation with Time Step Quantification in Terms of Langevin Dynamics, Phys. Rev. Lett. **84**, 163 (2000).

[31] C. S. Lent and D. J. Kirkner, The quantum transmitting boundary method, J. Appl. Phys. **67**, 6353 (1990).

[32] S. Tiwari, M. L. Van de Put, B. Sorée, and W. G. Vandenberghe, Carrier transport in two-dimensional topological insulator nanoribbons in the presence of vacancy defects, 2D Materials **6**, 025011 (2019).

[33] N. Metropolis and S. Ulam, The Monte Carlo method, J. Am. Stat. Assoc. **44**, 335 (1949), pMID: 18139350.

[34] See Supplemental Material at http://link.aps.org/supplemental/10.1103/PhysRevApplied.19.014040 for more information on the effect of pulse signals, the TI magnetization as a function of ribbon width, and the effect of pulse width on switching.

[35] M. Akram, H. LaBollita, D. Dey, J. Kapeghian, O. Erten, and A. S. Botana, Moire skyrmions and chiral magnetic phases in twisted CrX_3 (X = I, Br, and Cl) bilayers, Nano Lett. **21**, 6633 (2021), pMID: 34339218.

[36] L. N. Kapoor, S. Mandal, P. C. Adak, M. Patankar, S. Manni, A. Thamizhavel, and M. M. Deshmukh, Observation of standing spin waves in a van der Waals magnetic material, Adv. Mater. **33**, 2005105 (2021).

[37] D. Zhong, K. L. Seyler, X. Linpeng, R. Cheng, N. Sivadas, B. Huang, E. Schmidgall, T. Taniguchi, K. Watanabe, M. A. McGuire, W. Yao, D. Xiao, K.-M. C. Fu, and X. Xu, Van der Waals engineering of ferromagnetic semiconductor heterostructures for spin and valleytronics, Sci. Adv. **3**, e1603113 (2017).